Rare Metal Materials and Engineering
Volume 53, Issue 5, May 2024
Available online at www.rmme.ac.cn

Science Press

Cite this article as: Luo Chunyang, Xu Liujie, Shen Huahai, et al. Analysis of Irradiation Effects on Carbide Ceramics and Oxide Ceramics by SRIM[J]. Rare Metal Materials and Engineering, 2024, 53(05): 1245-1251. DOI: 10.12442/j.issn.1002-185X.20230777.

ARTICLE

Analysis of Irradiation Effects on Carbide Ceramics and Oxide Ceramics by SRIM

Luo Chunyang[1], Xu Liujie[1], Shen Huahai[2], Li Xiuqing[3], Wei Shizhong[1,3]

[1] National Joint Engineering Research Center for Abrasion Control and Molding of Metal Materials, Henan University of Science and Technology, Luoyang 471003, China; [2] Institute of Nuclear Physics and Chemistry, China Academy of Engineering Physics, Mianyang 621900, China; [3] Henan Key Laboratory of High Temperature Structural and Functional Materials, Henan University of Science and Technology, Luoyang 471003, China

Abstract: Dispersion strengthening plays an important role in improving the properties of alloys. The stability of carbide and oxide ceramics, as commonly used dispersion-reinforced particles, is important for alloys applied in nuclear reactors serving in harsh environments, so it is of great significance to study the radiation resistance of SiC, TiC, ZrC, Al_2O_3, Y_2O_3 and ZrO_2. The effects of different energies and different types of incident ions on different materials were simulated by SRIM program, and the irradiation damage of zirconia at different irradiation doses was analyzed. Results show that with the increase in incident ion energy, the distribution of the incident ions in the target material tends to be uniform and normal, and the stop position of the incident ions and the damage depth of the target material increase. The damage to the target material is different under different types of incident ion, which is not conducive to the radiation resistance comparison of the materials. Under the same irradiation conditions, the distribution of incident ions is consistent regardless of the increase in irradiation dose, but irradiation damage is accumulated until saturation. Among these six substances, zirconium oxide and zirconium carbide have better radiation resistance. The irradiation properties of zirconium oxide were verified by carbon ion irradiation experiments for tungsten alloy reinforced by zirconium oxide at 700 °C.

Key words: SRIM; ion irradiation; carbide and oxide ceramics; incident particles

Nuclear energy offers a solution to energy problems of increasingly short fossil energy sources. In nuclear fusion reactors, the service environment for plasma facing materials is harsh, and plasma facing materials are subjected to ion irradiation, neutron irradiation and high thermal loads. Under the action of multi-field coupling, the microstructure and surface morphology of plasma facing materials change, resulting in large changes in their mechanical and thermal properties, which affect the stable operation of the reactor[1–2]. Tungsten is considered as one of the most promising plasma facing materials because of its high melting point, good thermal conductivity, low sputtering yield and excellent thermal shock resistance[3–6]. However, tungsten has disadvantages such as high brittleness, high ductile-brittle transition temperature and low recrystallization temperature[7–9]. One of the current effective methods to improve the brittleness of tungsten is the addition of second-phase particles, which improve the strength and toughness of tungsten by hindering grain growth and refining grains to improve its brittleness. Commonly used second-phase particles include oxide particles (aluminum oxide[10], yttrium oxide[11], zirconium oxide[12]) and carbides (silicon carbide, titanium carbide[13], zirconium carbide[14]).

In principle, interfaces such as grain boundaries can absorb and annihilate irradiation-induced defects (gaps and vacancies) and reduce the accumulation of irradiation defects, thereby improving the irradiation resistance of the material. This mechanism was firstly demonstrated by Bai et al[15] using atomic simulations, where irradiation-generated defects are absorbed by grain boundaries and then re-emitted from the boundaries and vacancies in the matrix are eliminated, resulting in improved irradiation resistance. Recently, Wei et al[16] suggested that the effect of grain boundaries on

Received date: November 30, 2023
Foundation item: National Natural Science Foundation of China (U2004180); National Key Research and Development Program of China (2020YFB2008400)
Corresponding author: Xu Liujie, Ph. D., Professor, National Joint Engineering Research Center for Abrasion Control and Molding of Metal Materials, Henan University of Science and Technology, Luoyang 471003, P. R. China, E-mail: wmxlj@126.com

Copyright © 2024, Northwest Institute for Nonferrous Metal Research. Published by Science Press. All rights reserved.

improving irradiation resistance is manifested in the fracture and migration of grain boundaries by observing the changes of alumina grain boundaries during electron irradiation by in situ electron microscope. The addition of the second-phase can significantly reduce the grain size of tungsten, increase the grain boundary density, improve the hardness and strength of tungsten-based materials and lower the ductile-brittle transition temperature, thus improving the mechanical properties of tungsten. The addition of the second-phase improves the radiation resistance of tungsten-based materials, and reduces the density, size and expansion rate of dislocation rings induced by radiation.

There are still relatively few studies on the irradiation resistance of these second-phases. The exposure of the second-phase materials to the irradiation environment leads to the generation, migration and aggregation of irradiation-induced defects, resulting in the deterioration of their mechanical and thermal properties, which ultimately affects the overall properties of the tungsten-based materials. Irradiation damage leads to the transformation of SiC from crystalline to amorphous and decrease in density, hardness from 38.7 GPa to 21 GPa and elastic modulus from 528 GPa to 292 GPa[17]. Through neutron irradiation experiments on TiC_x (x=0.26, 0.66, 0.72), Matsui et al[18] found that the resistivity increases almost linearly with increasing neutron dose except at the beginning of irradiation. The higher the carbon content, the higher the damage rate of TiC. ZrC materials are also subjected to volume expansion during irradiation. The effect of irradiation on the physical properties of $ZrC_{0.98}$ was firstly reported by Andrievskii et al[19] and ZrC was irradiated at 425 and 1780 K with a flux of 1.5×10^{20} ion/cm^2 of fast neutrons. As the irradiation temperature increases, the material density shows a decreasing trend and the lattice parameters change. It is found that the microhardness of ZrC increases significantly after particle irradiation, especially at low temperatures. In contrast, monoclinic zirconia undergoes the same phase transition from monoclinic to tetragonal under ion irradiation environment. It has been reported that zirconia nanoparticles embedded in SiO_2 undergo phase transformation under Xe ion irradiation at 1 MeV[20], while in bulk zirconia, no phase transformation occurs even under high dose irradiation of 110 dpa[21]. Therefore, it is of interest to study the irradiation resistance of carbides and oxides added as a second-phase.

The purpose of this study is to explore the irradiation damage mechanism of different second-phases under the same irradiation conditions. In order to achieve this goal, the damage of gold ions on alumina, yttria, zirconia, silicon carbide, titanium carbide and zirconium carbide at different incident energies was simulated by SRIM software, and the energy loss percentage of gold ions in different materials was analyzed. Combined with the relevant irradiation experiments, the irradiation damage effects of different additives were analyzed, which provides reference for the subsequent corresponding work.

1 Computation Details

The irradiation effects of gold ions of different energies on alumina, yttria, zirconia, silicon carbide, titanium carbide and zirconium carbide were simulated by SRIM software[22]. The detailed calculation with total damage cascade algorithm was used for SRIM. The number of incident gold ions was 10 000, and the energy range of incident ion ranged from 0.01 MeV to 10 MeV. Carbon ions and gold ions were used as irradiating ions to explore the irradiation damage effect of different irradiating ions on zirconia; the incident ion energy was 3 MeV and the number of incident ions was 10 000. The off-site valve energy is the key parameter for the irradiation damage simulation, and the parameters used in the simulation were determined from the relevant literatures, as shown in Table 1.

The W-1.5% ZrO_2 alloy prepared by the azeotropic distillation method and high-temperature sintering (2700 °C) combined with high-temperature rotary swaging (1500 °C) was subjected to high-temperature vacuum annealing at 1400 °C, followed by carbon ion irradiation at 700 °C. The incident energy of carbon ion was 3 MeV, the intensity of ion beam was stabilized at 2.5 nA, and the irradiation doses were 1.7×10^{15}, 3.4×10^{15}, 6.8×10^{15}, 1.4×10^{16} ions/cm^2. The damage of zirconia located on the surface of W-1.5% ZrO_2 alloy after ion irradiation was observed by transmission electron microscopy (TEM).

2 Results and Discussion

2.1 Effect of irradiation energy

When an incident ion with energy irradiates the alloy materials, the alloy atoms block the motion of the incident ion mainly in the form of nuclear collisions and electron collisions, which are nuclear blocking and electron blocking, respectively. The electron blocking capability increases gradually with the increase in ion energy, and the nuclear blocking capability increases linearly at first and then decreases gradually after reaching the maximum value[28–29]. At low energy, the nuclear blocking capability is dominant. In the mid-energy region, the electron blocking capability is equally important as the nuclear blocking capability. In the high-energy region, the electron blocking capability is dominant,

Table 1 Simulation parameters for six materials

Material	SiC		TiC		ZrC		Al_2O_3		Y_2O_3		ZrO_2	
Density/g·cm^{-3}	3.2		4.93		6.7		4.0		5.01		6.10	
Threshold displacement energy/eV	Si	C	Ti	C	Zr	C	Al	O	Y	O	Zr	O
	35	20	40	30	50	30	18	76	25	28	40	40
Ref.	[23]		[24]		[24]		[25]		[26]		[27]	

and the nuclear blocking capability is minimal. Fig. 1 shows the nuclear blocking capability and electron blocking capability of different materials at different incident energies. Among these materials, SiC exhibits high electron blocking capability and nuclear blocking capability at the same energy, followed by alumina and titanium carbide.

Fig. 2 shows the relationship between ion energy loss and incident energy for different materials. It can be seen that with the increase in the incident ion energy, the percentage of ionization energy loss gradually increases, and the energy consumed by vacancy formation always keeps a small percentage. This is consistent with the variation of the nuclear blocking principal and the electron blocking principal. In the low-energy stage, the incident ion is blocked by the target atom, and the energy transferred to the atom is not enough to cause the atom to ionize, and finally consumed in the form of phonons. In the high-energy stage, the incident ion is transmitted to the impacted atom and the remaining energy after the collision still supports the continuous movement and collision of the atom or ion, thus reducing the percentage of phonon energy loss. The energy of the incident ion increases, but the ionization energy loss of SiC always keeps the highest percentage among these materials.

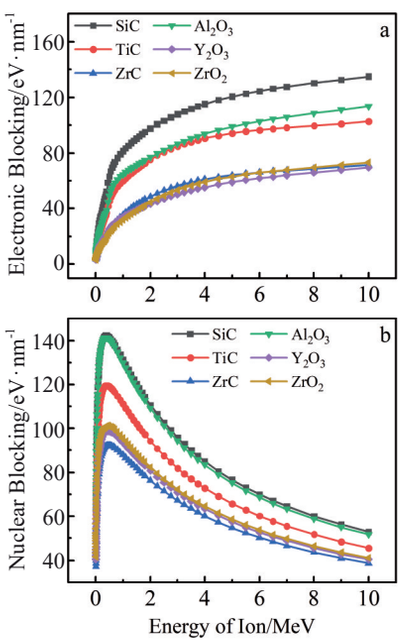

Fig.1 Relationship between the stopping power and the energy of the incident ion: (a) electronic blocking capability and (b) nuclear blocking capability

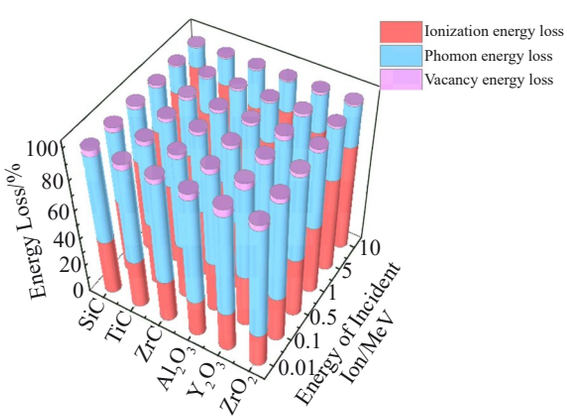

Fig.2 Ion energy loss in different materials versus incident ion energy

Fig. 3 shows the relationships among ion range, concentration distribution and ion energy. It can be seen from Fig.3a and 3b that the incident ion range increases linearly with increasing the ion energy. The range of incident ion in yttrium oxide keeps the maximum. The distribution of incident ions within the material is normal, and it does not change significantly with energy. The ion distribution in silicon carbide, titanium carbide and aluminum oxide tends to be narrow in height, and shows a trend of short-range and high damage. Zirconium carbide, yttrium oxide and zirconium oxide show long-range low ion concentrations, among which yttrium oxide is the most obvious. Fig.3c and 3d show the distributions of gold ions in the target when the ion energy is 0.1 and 10 MeV, respectively. At different energies, the distribution of the incident ions shows a normal distribution. With increasing the depth, the ion concentration increases slowly, then increases sharply to the maximum value, and then decreases sharply to 0. When the ion energy increases from 0.1 MeV to 10 MeV, the ion distribution depth increases, but the maximum concentration decreases. According to Fig. 1, when the incident ion energy reaches 10 MeV, it is mainly the electron blocking that plays a major role, and the direction of motion of the ions changes slightly after incidence, resulting in an increase in the depth of incidence. In the case that the total incident ions remain unchanged, the ion distribution shows a high narrow shape distribution. Alumina, silicon carbide and titanium carbide always keep a high concentration, and they have a more prominent vertical distribution than other substances. At the same time, the ions in zirconium carbide and zirconium oxide have similar range and concentration distributions, which may be related to zirconium atoms.

Fig. 4 shows the number of vacancies generated within the material after the incident of 10 000 ions. It can be found that there is little difference in the number of vacancies generated by various materials in the low-energy region. With increasing the energy, the number of vacancies produced in yttrium oxide increases rapidly. When the ion energy reaches 10 MeV, the number of vacancies in yttrium oxide is more than 10 000 compared to other materials, and there is little difference in other materials.

2.2 Different incident ions

Zirconia was used as a research object to analyze the off-site damage caused by light mass heavy C ions and heavy mass heavy gold ions to zirconia based on SRIM simulation results.

Fig. 5 shows the stopping power of zirconia to different incident ions. The results show that this material exhibits different blocking capacities to different incident ions. The

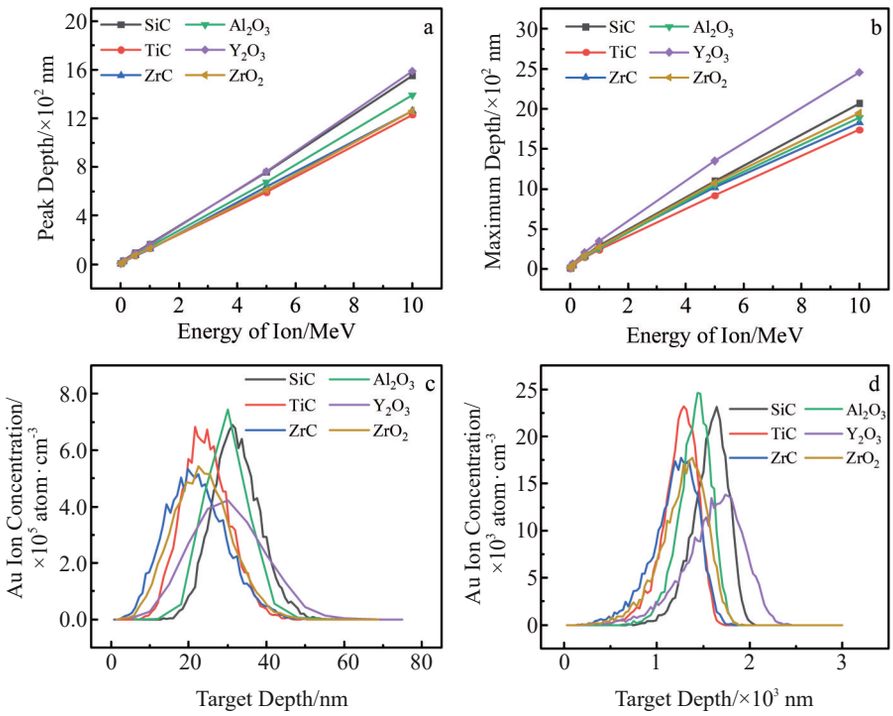

Fig.3 Relationships among ion range, concentration distribution and ion energy: (a) peak depth, (b) maximum depth, (c) ion concentration distribution at ion energy of 0.1 MeV, and (d) ion concentration distribution at ion energy of 10 MeV

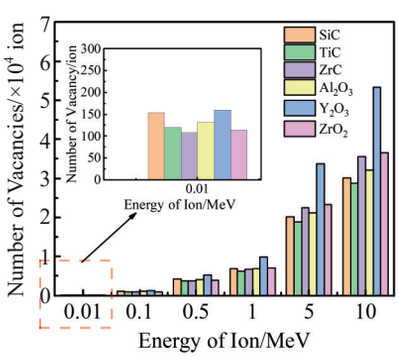

Fig.4 Number of vacancies generated within the material versus ion energy

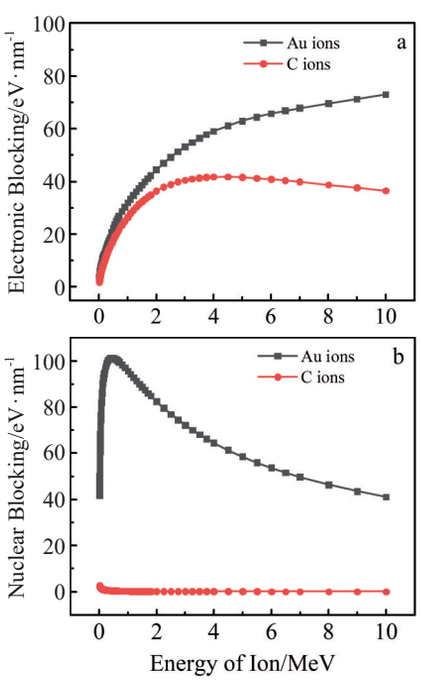

Fig.5 Stopping power of zirconium oxide to carbon and gold ions versus energy: (a) electron blocking capability and (b) nuclear blocking capability

ability of atoms to stop gold ions of different energies has been discussed in the previous chapter. For carbon ions, the electron blocking ability increases with the increase in energy in the low-energy region, which reaches a maximum value around 3 MeV and then decreases slowly. The nuclear blocking capability of zirconium oxide for carbon ions decreases with increasing the energy and then stabilizes. Comparing these two kinds of ions, it can be found that the blocking ability of zirconia to gold ions is much higher than that to carbon ions.

Fig. 6 shows the energy loss of carbon and gold ions in zirconia at 3 MeV. Similarly, no matter what the incident ions are, the energy consumed by vacancy formation is extremely low, while the percentage of the carbon ion is almost invisible. The reason for this difference is that the ionization energy loss and phonon energy loss account for a certain proportion in the energy loss of the gold ion, while the energy loss of the carbon ion is mainly ionization energy loss, reaching over 90%. The collision energy loss of carbon ions with zirconia nuclei is less, and the probability of atomic dislocation is lower than that of gold ion incidence, indicating that the damage caused

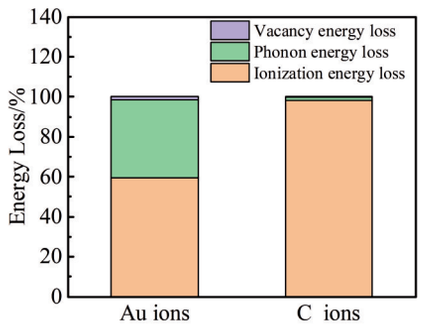

Fig.6 Energy loss of gold ions and carbon ions

by gold ions is more serious under the same conditions.

Fig. 7 shows the concentration distribution of carbon and gold ions in the material and the resulting vacancy distribution. Both of them are consistent. The gold ions consume a lot of energy on the surface of the material, and the nuclear collision reaction is intense, resulting in a large number of vacancies in the near-surface area of the material. Compared with the gold ions, the vacancy formation rate caused by carbon ions is extremely low, no more than 1/atom. Once again, the damage caused by gold ions is higher than that caused by carbon ions.

2.3 Carbon ion irradiation experiments of zirconium oxide

The tungsten alloy reinforced by zirconia particles was subjected to carbon ion irradiation experiments at 700 °C. Irradiation damage of zirconium oxide in tungsten alloy can be observed. The microstructure of zirconia particles with almost no omission on the surface of the sample is observed,

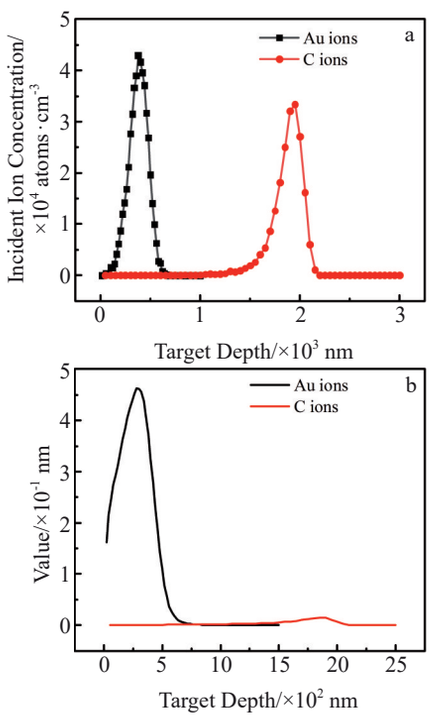

Fig.7 Concentration distribution (a) and vacancy formation rate (b) of carbon and gold ions

and the irradiation damage of zirconia caused by different doses of carbon ion irradiation is analyzed. Based on the simulation results of SRIM, combined with Eq. (1) [30], the irradiation damage of zirconia at different irradiation doses is calculated, which is expressed as dpa.

$$\mathrm{dpa}=\frac{\mathrm{Vacancies}}{\mathrm{ions}\times\mathrm{nm}}\times\left[\frac{10^{8}\left(\frac{\mathrm{nm}}{\mathrm{cm}}\right)\times\mathrm{Fluence}\left(\frac{\mathrm{ions}}{\mathrm{cm}^{2}}\right)}{\left(\frac{\mathrm{atoms}}{\mathrm{cm}^{2}}\right)}\right]$$

where atoms/cm^2 denotes the atomic density of the material, ions/cm^2 denotes the ion irradiation dose and vacancies/(ions ×nm) denotes the damage efficiency. The data are obtained from the SRIM simulation results of vacancy file.

Fig.8 shows the distribution of irradiation damage in zirconia at different irradiation doses. Combined with the discussions in the first two sections, at the same energy, the blocking principle of the target atom to the incident ion is certain. As can be seen from Fig.8, the distribution of irradiation damage in zirconia along the incident direction at different irradiation doses follows the same trend, i. e., firstly increasing slowly, then reaching a maximum and finally sharply decreasing. The peak position of the irradiation damage is 1.85 μm, and the peak depth does not change with increasing the dose. When the depth reaches 2.1 μm, the damage caused by the incident ions can be almost ignored. The maximum irradiation damages corresponding to these four irradiation doses are 0.32, 0.63, 1.26 and 2.6 dpa, respectively.

As shown in Fig.9a, we selected particles that hardly escape from the surface of the sample and can be irradiated by ions for research. According to the low-power transmission photos, it can be found that the white particles are spherical or nearly spherical, and distributed at the grain boundaries or within the grains of the matrix. Fig.9b shows the diffraction points of the white particles which have been calibrated. The white particles are cubic zirconia, which do not undergo phase transition and attenuation. This phenomenon is different from the zirconia embedded in the matrix. As mentioned earlier, the latter is more likely to undergo phase transition, which may be related to the differences of radiation environment. The existence of yttria stabilizer in zirconia weakens the phase transition trend. Fig.9c–9f show the high magnification TEM images of zirconia at different irradiation doses. It is obvious

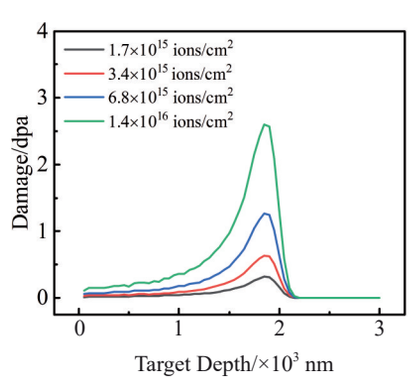

Fig.8 Irradiation damage in zirconia as a function of irradiation dose

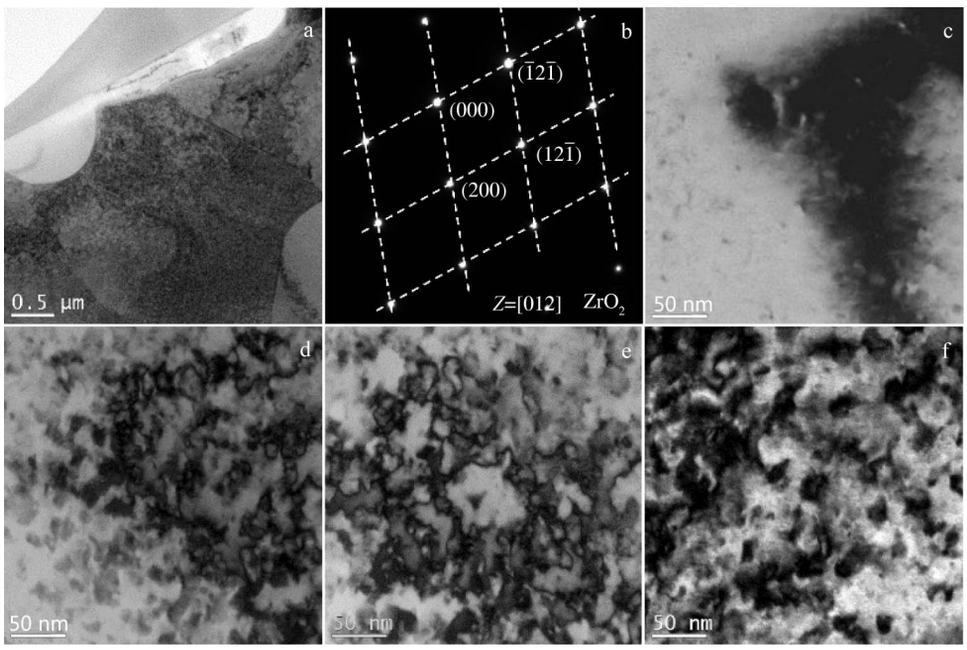

Fig.9 TEM images (a) and diffraction spots (b) of zirconia after carbon ion irradiation; high magnification TEM images of zirconia at different irradiation doses: (c) 0.32 dpa, (d) 0.63 dpa, (e) 1.26 dpa, and (f) 2.6 dpa

that dislocation loops are distributed in the zirconia grains. The number of dislocation loops in zirconia particles is very small, but the size of dislocation loops is very large. It can be directly seen that the density and diameter of dislocation ring increase with increasing the irradiation dose, and the diameter can reach several tens of nanometers.

From the analysis of the previous subsections, it can be found that under the same doses of incident ions, the damage caused by different incident ion energies is different, but the overall trend is relatively consistent. ZrC and ZrO_2 show a relatively consistent damage trend, and Y_2O_3 shows a weak anti-radiation ability. Under the same incident conditions, the damage depth of Y_2O_3 is the largest. When the energy transferred by the incident ions to Y_2O_3 is greater than the threshold value, Y_2O_3 undergoes a phase transition from cubic phase to monoclinic phase, and the smaller the grain size, the easier the phase transition will occur[31]. Among the three carbides, it can be seen from the ion distribution and ion range that the anti-irradiation ability of SiC is weak, which may be due to different electronic structures. The chemical bonds between Ti-C and Zr-C is a mixture of covalent bonds, metallic bonds and ionic bonds, while Si-C is mainly covalent bonds[32]. Under the same irradiation conditions, the irradiation damage caused by different incident ions to the target is also very different, which brings great difficulties to study on the irradiation resistant performance of different substances.

Modern research has found that SiC[17,33], TiC[18,34], ZrC[19,35], Al_2O_3[36], Y_2O_3[31] and ZrO_2[20–21] will undergo attenuation or phase transformation under ion irradiation, resulting in changes of their organizational characteristics. As a substance that needs to face the plasma reaction directly, its stability is very important. Therefore, it is of great significance to study the mechanism of radiation damage and to compare radiation resistance.

3 Conclusions

1) Under the same incident conditions, with the increase in irradiation ion energy, the distribution of the incident ions within the target tends to be uniform and normal. However, the stopping depth of the incident ions gradually increases and tends to be stable, which is related to the stopping ability of the target atoms.

2) Under the same incident conditions, with the increase in incident ion dose, the distribution of incident ions within the target remains unchanged, and irradiation defects gradually accumulate, leading to greater damage, which is consistent with the experimental results of irradiation on zirconia.

3) Under the condition of the same irradiation ion energy, the damage of different incident ions to the target is very different. Therefore, a database of radiation effects should be established as soon as possible, so as to compare the irradiation ability of materials and to select materials suitable for nuclear use.

4) The SRIM simulations reveal that among the six substances including SiC, TiC, ZrC, Al_2O_3, Y_2O_3 and ZrO_2, zirconium carbide and zirconium oxide show better resistance to irradiation and the simulation results for these two substances are similar, which may be related to the Zr binding mode and needs to be investigated and explained by atomic level experiments.

References

1 Gauthier E, Dumas S, Matheus J *et al*. *Journal of Nuclear Materials*[J], 2005, 337–339(1): 960

2 Zhao Yiluo, Lei Ming, Zhang Xu *et al*. *Rare Metal Materials and Engineering* [J], 2021, 50(9): 3399 (in Chinese)
3 Pitts R A, Carpentier S, Escourbiac F *et al. Journal of Nuclear Materials*[J], 2011, 415(1): S957
4 Neu R, Rohde V, Geier A *et al. Journal of Nuclear Materials*[J], 2001, 290: 206
5 Bao Hongwei, Li Yan, Ma Fei. *Rare Metal Materials and Engineering* [J], 2022, 51(3): 1100 (in Chinese)
6 Ji Suyan, Chong Fali, Liao Kai *et al*. *Rare Metal Materials and Engineering* [J], 2021, 50(10): 3714 (in Chinese)
7 Tanabe T, Akiba M, Ueda Y *et al. Fusion Engineering and Design*[J], 1998, 39: 275
8 Rieth M, Boutard J L, Dudarev S L. *Journal of Nuclear Materials*[J], 2011 417(1–3): 463
9 Jiang Yan, Chen Min, Jiang Zhiqiang. *Rare Metal Materials and Engineering*[J], 2023, 52(2): 623 (in Chinese)
10 Li B Q, Sun Z Q, Hou G L *et al. Inorganic Chemistry Frontiers*[J], 2017, 692: 420
11 Hu W Q, Dong Z, Ma Z Q *et al. Inorganic Chemistry Frontiers*[J], 2020, 7(3): 659
12 Li Z, Xu L J, Wei S Z *et al. Journal of Alloys and Compounds*[J], 2018, 769: 694
13 Li L Q, Fan J L, Tian J M *et al. Materials Science and Engineering A*[J], 2021, 819: 141
14 Lang E, Madden N, Smith C *et al. International Journal of Refractory Metals and Hard Materials*[J], 2018, 75: 279
15 Bai X M, Voter A F, Hoagland R G *et al. Science*[J], 2010, 327(5973): 1631
16 Wei J K, Feng B, Tochigi E *et al. Nature Communications*[J], 2022, 13(1): 1455
17 Snead L L, Zinkle S J, Hay J C *et al. Nuclear Inst and Methods in Physics Research B*[J], 1998, 141(1): 123
18 Matsui H, Guinan M W, Iida T *et al. Journal of Nuclear Materials*[J], 1985, 133(C): 718
19 Andrievskii R A. *Physics of Metals and Metallography*[J], 2010, 110(3): 229
20 Meldrum A, Boatner L A, Ewing R C. *Physical Review Letters*[J], 2002, 88(2): 025503
21 Fleischer E L, Norton M G, Zaleski M A *et al. Journal of Materials Research*[J], 1991, 6(9): 1905
22 Ziegler J F, Biersack J P, Littmark U. *The Stopping and Range of Ions in Solids*[M]. New York: Pergamon, 1985
23 Devanathan R, Weber W J. *Journal of Nuclear Materials*[J], 2000, 278(2): 258
24 Pellegrino S, Trocellier P, Thomé L *et al. Nuclear Instruments and Methods in Physics Research Section B*[J], 2017 454: 61
25 Parkin Don M, Coulter C. *Journal of Nuclear Materials*[J], 1981, 101(3): 261
26 Kazuki N, Hikari F, Jan E *et al. Journal of Nuclear Materials*[J], 2020, 537(15): 152244
27 Sickafusa K E, Matzkeb H J, Hartmanna T H. *Journal of Nuclear Materials*[J], 1999, 274(1–2): 66
28 Marmier P, Sheldon E. *Physics of Nuclei and Particles*[M]. New York: Academic Press Inc, 1969: 23
29 Evens D. *The Atomic Nucleus*[M]. New York: McGraw-Hill Inc, 1955: 18
30 Chang J, Cho J Y, Gil C S *et al. Nuclear Engineering & Technology*[J], 2014, 46(4): 475
31 Hemon S, Berthelot A, Dufour C H *et al. The European Physical Journal B*[J], 2001, 19: 517
32 Jiang M, Xiao H Y, Zhang H B *et al*. *Acta Materialia*[J], 2016, 110: 192
33 Yutai K, Lance L S, Izabela Szlufarsk *et al*. *Current Opinion in Solid State and Materials Science*[J], 2012, 16: 143
34 Hojou K, Otsu H, Furuno S *et al. Nuclear Instruments and Methods in Physics Research B*[J], 1997, 127: 203
35 Gosset D, Dolle M, Simeone D *et al. Journal of Nuclear Materials*[J], 2008, 373: 123
36 Ghyngazov S A, Koval N N, Kostenko V A. *Russian Physics Journal*[J], 2021, 64: 367

利用 SRIM 分析辐照对碳化物和氧化物陶瓷的影响

罗春阳[1]，徐流杰[1]，申华海[2]，李秀青[3]，魏世忠[1,3]

(1. 河南科技大学 金属材料磨蚀控制与成型国家联合工程研究中心，河南 洛阳 471003)

(2. 中国工程物理研究院 核物理与化学研究所，四川 绵阳 621900)

(3. 河南科技大学 高温结构与功能材料河南省重点实验室，河南 洛阳 471003)

摘　要：弥散强化在改善合金性能方面发挥着重要作用，而碳化物和氧化物陶瓷作为常用的弥散强化颗粒，其稳定性对于应用于恶劣环境的核反应堆中的合金非常重要，因此研究SiC、TiC、ZrC、Al_2O_3、Y_2O_3和ZrO_2的抗辐射性具有重要意义。利用SRIM程序模拟了不同能量、不同类型的入射离子对不同材料的影响，分析了不同辐照剂量下氧化锆的辐照损伤。结果表明，随着入射离子能量的增加，入射离子在靶材中的分布趋于均匀，入射离子的停止位置和靶材的损伤深度有所增加。入射离子的种类不同，对靶材的损伤程度也大不相同，不利于对比材料的抗辐射能力。在相同的辐照条件下，入射离子的分布随辐照剂量的增加保持不变，但辐照损伤会不断累积直至饱和。在6种物质中，氧化锆和碳化锆的抗辐射性能较好。对氧化锆增强的钨合金在700 ℃进行碳离子辐照实验，发现氧化锆具有良好的辐照性能。

关键词：SRIM；离子辐照；碳化物和氧化物；入射粒子

作者简介：罗春阳，男，1997年生，硕士生，河南科技大学金属材料磨蚀控制与成型国家联合工程研究中心，河南 洛阳 471003，E-mail：luochunyang2020@163.com